

Overlapping Schwarz Preconditioners for Pose-Graph SLAM in Robotics

Stephan Köhler, Oliver Rheinbach, Yue Xiang Tee, and Sebastian Zug

Abstract We investigate the application of the additive overlapping Schwarz domain decomposition method as a preconditioner for the large sparse linear systems arising in graph-based nonlinear least-squares problems, specifically the pose-graph optimization back-end in Simultaneous Localization and Mapping (SLAM) in robotics. A brief introduction to both SLAM and domain decomposition preconditioners is given, followed by a description of the nonlinear least-squares formulation, its linearization, and the resulting matrix structure, making the paper accessible to readers without prior knowledge of either field. Numerical experiments for a simple model problem demonstrate the numerical scalability of the preconditioned conjugate gradient method to solve the linear systems resulting from Gauss–Newton linearization: Using the additive overlapping Schwarz preconditioner, the number of conjugate gradient iterations remains bounded independently of the problem size. We also show that a simplified SLAM problem can be interpreted as a finite element problem using linear elastic bars, highlighting the structural analogy to PDE discretizations and motivating the use of PDE-based preconditioners such as scalable domain decomposition preconditioners.

Stephan Köhler · Oliver Rheinbach · Yue Xiang Tee · Sebastian Zug
Faculty of Mathematics and Computer Science, Technische Universität Bergakademie
Freiberg, Akademiestr. 6, 09599 Freiberg.
e-mail: stephan.koehler@math.tu-freiberg.de, oliver.rheinbach@math.tu-freiberg.de, Yue-Xiang.Tee@math.tu-freiberg.de, Sebastian.Zug@informatik.tu-freiberg.de,

1 Introduction

Simultaneous Localization and Mapping (SLAM) addresses the problem of estimating a robot’s trajectory while simultaneously constructing a map of its environment. In large-scale scenarios such as long-term operation in outdoor environments, SLAM leads to very large sparse optimization problems derived from noisy sensor measurements. Solving these problems efficiently and robustly remains a major challenge, motivating the development of fast SLAM algorithms.

Preconditioning techniques have been proposed to accelerate the iterative solution of the large sparse linear systems that arise in graph-based SLAM, for instance when solving the normal equations in nonlinear least-squares methods such as Gauss–Newton or Levenberg–Marquardt. Different approaches have been explored in the literature. For instance, a subgraph-based preconditioner constructed from a sparse subgraph structure, such as a spanning tree, was proposed in [1] and later extended to incremental settings suitable for online SLAM in [2]. Block-Jacobi preconditioning and the direct solution of Schur complement systems are considered in [3]. Incomplete Cholesky factorizations have also been used as preconditioners for conjugate gradients applied to the sparse linear systems arising in Levenberg–Marquardt SLAM [4], where they are also compared to sparse direct solvers. In practical SLAM systems such as the `g2o` software library [5], the linear systems arising in pose graph optimization are typically solved using sparse direct Cholesky factorization (e.g., `CHOLMOD`). While iterative methods such as preconditioned conjugate gradients are also available, they typically employ computationally inexpensive preconditioners such as block-Jacobi or diagonal scaling.

However, many of these approaches do not exhibit numerical scalability as the problem size grows, i.e., the performance can deteriorate as the problem size increases. Indeed, as emphasized in the overview paper [6], the development of scalable SLAM methods remains a fundamental open challenge for achieving long-term autonomy in large environments.

In this paper, we will demonstrate numerically that domain decomposition preconditioners, specifically an additive overlapping Schwarz preconditioner, applied to a simple test problem in SLAM, can lead to a numerically scalable method, i.e., the number of preconditioned conjugate gradient iterations remains small and bounded independently of the problem size. Keeping the number of iterations small is important in practice, since large iteration counts may lead to loss of orthogonality in the conjugate gradient method in finite precision arithmetic.

We will first give a brief introduction to both SLAM and the overlapping Schwarz method. This is followed by a description of the mathematical formulation of the problem as well as the problem setting. We also present a very simple one-dimensional SLAM problem to illustrate the connections of SLAM to continuum mechanical problems discretized by the finite element method.

Finally, the convergence results for our the Schwarz preconditioner applied to a SLAM model problem in two dimensions are presented and discussed.

2 Simultaneous Localization and Mapping (SLAM)

In SLAM, the trajectory of a robot and a map of the environment are estimated simultaneously from noisy sensor measurements. The localization problem has been investigated since the 1990s, initially with a strong focus on filter-based approaches such as the extended Kalman filter; see, e.g., [7, 8, 9, 10]. With the growing interest in SLAM in recent years, several comprehensive surveys have been published. In particular, [6] provides an overview of the development of SLAM, while more recent surveys discuss the architecture of complete SLAM systems and modern sensor configurations [11, 12].

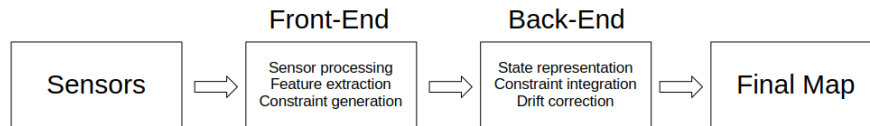


Fig. 1: Simplified flow chart of a complete SLAM system.

A SLAM system starts with the collection of data from sensors, and ends with the creation of a map, with which the robot is able to orient itself. This process can be briefly summarized as in Fig. 1.

A SLAM system typically consists of a front-end and a back-end. The front-end processes sensor data to estimate relative motion (odometry) between robot poses. The specific approach depends on the sensor modality, for example visual SLAM for camera-based systems [13] or LiDAR-based SLAM for laser sensors [14]. By extracting features and performing data association, the front-end produces measurement constraints that are passed to the back-end for global estimation.

Due to the inevitable accumulation of noise in sensor measurements, drift may accumulate over time. When the system revisits a previously observed location, additional constraints, known as *loop closures*, can be introduced, which allow the accumulated drift to be corrected.

The back-end estimates the robot states from the motion and measurement constraints. This can be achieved using either filter-based or graph-based methods. Filter-based methods estimate the current state of the system recursively by propagating and updating a probability distribution as new measurements arrive. In graph-based methods, robot poses, map variables, and measurements are represented as nodes connected by constraints

in a graph, and the most consistent global solution is computed by solving a nonlinear least-squares problem; see [15] for a tutorial. Efficient implementations of such formulations are provided by general graph-optimization frameworks such as g2o [5].

In this paper, after linearization, e.g., using Gauss–Newton, the ill-conditioned linear system is solved by a preconditioner Krylov method using an additive overlapping Schwarz preconditioner. This is described in more detail in the following sections.

2.1 Mathematical Formulation of Pose Graph SLAM in two dimensions

We describe the specific nonlinear least-squares problem underlying the numerical experiments formulated in classical terms of finite-dimensional nonlinear optimization.

In two-dimensional SLAM a *pose* represents the configuration of the robot in the plane. Here, it consists of a position vector and an orientation angle and is represented by

$$p = (x, y, \theta)^T \in \mathbb{R}^2 \times \mathbb{R}.$$

The orientation angle θ is defined modulo 2π . For numerical purposes, angles are always mapped to a fixed interval, e.g. $(-\pi, \pi]$.

Given two poses $p_i = (x_i, y_i, \theta_i)$ and $p_j = (x_j, y_j, \theta_j)$, their *relative pose* is defined as the configuration of p_j expressed in the local coordinate system of p_i .

Algebraically, the relative pose is given by the smooth nonlinear mapping $\Phi : \mathbb{R}^3 \times \mathbb{R}^3 \rightarrow \mathbb{R}^3$,

$$\Phi(p_i, p_j) = p_i^{-1} \circ p_j = \begin{pmatrix} R(\theta_i)^T (t_j - t_i) \\ \theta_j - \theta_i \end{pmatrix}, \quad (2.1)$$

where $t_i = (x_i, y_i)^T$ and

$$R(\theta_i) = \begin{pmatrix} \cos \theta_i & -\sin \theta_i \\ \sin \theta_i & \cos \theta_i \end{pmatrix}$$

denotes the rotation matrix associated with θ_i . The angle difference is again mapped to a fixed interval.

The problem data consist of relative pose measurements. For certain index pairs (i, j) , a measurement

$$\tilde{\Phi}_{ij} = (\delta \tilde{x}_{ij}, \delta \tilde{y}_{ij}, \delta \tilde{\theta}_{ij})^T \quad (2.2)$$

is given, represented by the edge $(i, j) \in E$ of the pose graph. This edge represents a (potentially noisy) observation of the relative pose between p_i and p_j , i.e., $\tilde{\Phi}_{ij} \approx \Phi(p_i, p_j)$. In our numerical experiments, two types of measurements are used:

- *Sequential measurements*, which connect consecutive poses and incremental motion.
- *Loop closure measurements*, which connect poses that are far apart in the sequence and introduce global coupling.

Loop closures occur whenever the robots recognizes a place it has already visited. They are important because they allow to correct the error accumulated on the robot's path. A loop closure is simply an additional constraint

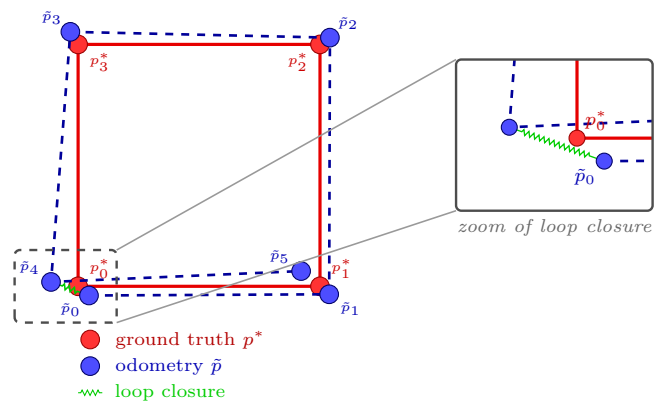


Fig. 2: Example for a SLAM problem; ground truth (red) and odometry data (blue); between the pose \tilde{p}_4 and \tilde{p}_0 is a loop closure edge (green)

between poses indicating that these poses should be the same; see Fig. 2. These constraints are treated in the same way as the other measurements, i.e., they participate in the least-squares adjustment and are not enforced exactly. However, each measurement is weighted using a diagonal (or symmetric positive definite) weight matrix with entries $W_{ij} \in \mathbb{R}^{3 \times 3}$, and, often, a higher weight is used for the loop closure measurements, indicating their high importance. Let us remark that we can set entry for the orientation in the weight matrix to zero if we are not interested in the robot's orientation at a loop closure.

For a given estimate $\tilde{\Phi}_{ij}$ for the relative pose $\Phi(p_i, p_j)$, the corresponding residual is defined as

$$r_{ij}(p_i, p_j) = \Phi(p_i, p_j) - \tilde{\Phi}_{ij}. \quad (2.3)$$

The rotational component of the residual is mapped to the principal interval to ensure continuity. The residual measures the discrepancy between the predicted relative pose $\Phi(p_i, p_j)$ and the measured relative pose $\tilde{\Phi}_{ij}$.

We model the SLAM problem by means of a pose graph $G = (V, E)$, where the vertex set $V := \{0, 1, \dots, N\}$ indexes the robot poses p_i , and the edge set $E \subset V \times V$ encodes relative pose measurements between pairs of poses.

2.2 Least-Squares Formulation

An edge $(i, j) \in E$ exists in our pose graph if p_i and p_j are consecutive poses, i.e., $j = i + 1$, or if the edge (i, j) represents a loop-closure constraint between p_i and p_j ; see Fig. 2.

The global least squares objective function is given by

$$\mathcal{J}(p_1, \dots, p_N) = \frac{1}{2} \sum_{(i,j) \in E} r_{ij}(p_i, p_j)^T W_{ij} r_{ij}(p_i, p_j). \quad (2.4)$$

Where W_{ij} is the weight matrix introduced in section 2.1. The objective function is invariant under global rigid transformations. The nonlinear least-squares problem is given by

$$\min_{(p_1, \dots, p_N) \in \mathbb{R}^{3N}} \mathcal{J}(p_1, \dots, p_N) \quad (2.5)$$

To remove the null space of the problem, one pose is fixed in our model problem.

Note that (2.5) can also be written as

$$\min_{(p_1, \dots, p_N) \in \mathbb{R}^{3N}} \frac{1}{2} \sum_{(i,j) \in E_{\text{odom}}} \|r_{ij}(p_i, p_j)\|_W^2 + \frac{1}{2} \sum_{(i,j) \in E_{\text{loop}}} \|r_{ij}(p_i, p_j)\|_W^2,$$

where E_{odom} represents all pairs (i, j) from the consecutive measurements, E_{loop} all pairs from the loop closure measurements, and $\|\cdot\|_{W_{ij}}$ the norm induced by the weight matrix W_{ij} .

From (2.1) it follows that the Jacobian of $\Phi(p_i, p_j)$ is given by

$$\begin{aligned}
& D\Phi(p_i, p_j) \\
&= \begin{pmatrix} \frac{\partial \Phi_1}{\partial x_i} & \frac{\partial \Phi_1}{\partial y_i} & \frac{\partial \Phi_1}{\partial \theta_i} & \frac{\partial \Phi_1}{\partial x_j} & \frac{\partial \Phi_1}{\partial y_j} & \frac{\partial \Phi_1}{\partial \theta_j} \\ \frac{\partial \Phi_2}{\partial x_i} & \frac{\partial \Phi_2}{\partial y_i} & \frac{\partial \Phi_2}{\partial \theta_i} & \frac{\partial \Phi_2}{\partial x_j} & \frac{\partial \Phi_2}{\partial y_j} & \frac{\partial \Phi_2}{\partial \theta_j} \\ \frac{\partial \Phi_3}{\partial x_i} & \frac{\partial \Phi_3}{\partial y_i} & \frac{\partial \Phi_3}{\partial \theta_i} & \frac{\partial \Phi_3}{\partial x_j} & \frac{\partial \Phi_3}{\partial y_j} & \frac{\partial \Phi_3}{\partial \theta_j} \end{pmatrix} \\
&= \begin{pmatrix} -\cos \theta_i & -\sin \theta_i & -\sin \theta_i(x_j - x_i) + \cos \theta_i(y_j - y_i) & \cos \theta_i & \sin \theta_i & 0 \\ \sin \theta_i & -\cos \theta_i & -\cos \theta_i(x_j - x_i) - \sin \theta_i(y_j - y_i) & -\sin \theta_i & \cos \theta_i & 0 \\ 0 & 0 & -1 & 0 & 0 & 1 \end{pmatrix},
\end{aligned}$$

where we dropped the arguments in the second row for simplicity. The gradient of \mathcal{J} can be written as

$$\nabla \mathcal{J}(p_1, \dots, p_N) = \begin{pmatrix} \nabla_{p_1} \mathcal{J}(p_1, \dots, p_N) \\ \vdots \\ \nabla_{p_N} \mathcal{J}(p_1, \dots, p_N) \end{pmatrix} \in \mathbb{R}^{3N},$$

where

$$\begin{aligned}
\nabla_{p_i} \mathcal{J}(p_1, \dots, p_N) &= \begin{pmatrix} \frac{\partial \mathcal{J}}{\partial x_i}(p_1, \dots, p_N) \\ \frac{\partial \mathcal{J}}{\partial y_i}(p_1, \dots, p_N) \\ \frac{\partial \mathcal{J}}{\partial \theta_i}(p_1, \dots, p_N) \end{pmatrix} \\
&= \sum_{\substack{(k, \ell) \in E, \\ k=i \text{ or } \ell=i}} D\Phi(p_k, p_\ell)^T W_{k\ell} r_{k\ell}(p_k, p_\ell).
\end{aligned} \tag{2.6}$$

The Hessian H of \mathcal{J} can be written as

$$H = \begin{pmatrix} H_{p_1, p_1} & \dots & H_{p_1, p_N} \\ \vdots & & \vdots \\ H_{p_N, p_1} & \dots & H_{p_N, p_N} \end{pmatrix},$$

where H_{p_i, p_j} is given by

$$\begin{aligned}
H_{p_i, p_j} &= \nabla_{p_i, p_j}^2 \mathcal{J}(p_1, \dots, p_N) \\
&= \underbrace{\sum_{\substack{(k, \ell) \in E, \\ k \in \{i, j\} \text{ and } \ell \in \{i, j\}}} D\Phi(p_k, p_\ell)^T W_{k\ell} D\Phi(p_k, p_\ell)}_{\text{Gauss-Newton approximation}} + B_{p_i, p_j},
\end{aligned} \tag{2.7}$$

where the matrix B_{p_i, p_j} contains the second order derivatives of $\Phi(p_i, p_j)$. From (2.7) it follows that

$$H = H_{\text{GN}} + B,$$

where H_{GN} refers to the Gauss–Newton approximation of H . Here, B refers to the second order derivatives of Φ , which are neglected in Gauss–Newton.

To derive a more compact matrix notation often used in the literature, let

$$r(p) = \begin{pmatrix} r_{i_1 j_1}(p_{i_1}, p_{j_1}) \\ \vdots \\ r_{i_m j_m}(p_{i_m}, p_{j_m}) \end{pmatrix} \in \mathbb{R}^{3m}$$

denote the stacked residual vector containing all edge residuals, where $m = |E|$ is the number of edges in the pose graph. Furthermore, let

$$W = \text{diag}(W_{i_1 j_1}, \dots, W_{i_m j_m})$$

be the block diagonal matrix collecting all weight matrices. Then the objective function (2.4) can be written as

$$\mathcal{J}(p) = \frac{1}{2} r(p)^T W r(p).$$

Let

$$J(p) = \frac{\partial r(p)}{\partial p}$$

denote the Jacobian of the stacked residual vector. Then the gradient of \mathcal{J} can be written as

$$\nabla \mathcal{J}(p) = J(p)^T W r(p).$$

Finally, the Gauss–Newton approximation of the Hessian is given by

$$H_{\text{GN}}(p) = J(p)^T W J(p). \quad (2.8)$$

If the weight matrices W_{i_j} are symmetric positive definite and the natural null space of the problem is removed (e.g. by fixing one pose), then H_{GN} is symmetric positive definite, and the conjugate gradient method is applicable.

Since, throughout this paper, we are using Gauss–Newton, we may also drop the subscript GN from H_{GN} .

3 Overlapping Schwarz Domain Decomposition Preconditioners

The general concept of domain decomposition methods (DDM) is based on divide-and-conquer: A large problem is decomposed into multiple smaller, more manageable subproblems that can be solved separately and in parallel. A comprehensive introduction to DDM can be found in [16, 17]. DDM are typically accelerated by Krylov methods such as conjugate gradients.

The divide-and-conquer approach makes DDM very attractive for the parallel solution of large ill-conditioned problems. This motivated significant research activity on the usage of DDM in large problems from computational fluid mechanics [18], structural mechanics [19, 20], or coupled problems problems [21, 22, 23].

Although DDM were originally developed for the solution of large systems from the discretization of partial differential equations, e.g., by finite elements, the underlying ideas can also be formulated algebraically.

Let $A \in \mathbb{R}^{n \times n}$ be symmetric positive definite. Assume that the index set $\{1, \dots, n\}$ is covered by overlapping subsets $\mathcal{I}_1, \dots, \mathcal{I}_N$. For each subdomain i , a restriction operator

$$R_i : \mathbb{R}^n \rightarrow \mathbb{R}^{n_i} \quad (3.1)$$

extracts the components belonging to \mathcal{I}_i .

The restriction operators R_i can be interpreted as Boolean extraction matrices selecting the degrees of freedom belonging to the index set \mathcal{I}_i . In particular, each R_i is a submatrix of the identity matrix that extracts the components of a global vector associated with the poses in the i -th subdomain.

In the context of pose graph SLAM, the index sets \mathcal{I}_i correspond to subsets of robot poses, so that each subdomain represents a contiguous segment of the robot trajectory.

Overlapping Schwarz methods are a subclass within DDM, which use overlapping subdomains. For additive one-level overlapping Schwarz, local corrections are computed on each subdomain and then combined additively to a global approximate solution; see (3.2). This method then takes the role of the preconditioner in a Krylov method such as conjugate gradients.

The amount of overlap is a parameter in overlapping Schwarz methods. The case where the overlap is restricted to a single layer of degrees of freedom adjacent to the interface between neighboring subdomains is referred to as *minimal overlap*. Here, the interface denotes the common boundary between two neighboring subdomains. Increasing the overlap generally improves the convergence of the method, but also increases the computational cost of the local subdomain solves.

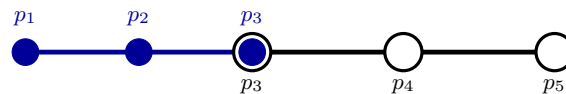


Fig. 3: Illustration of a robot trajectory decomposed into two overlapping subdomains p_1 - p_2 - p_3 and p_3 - p_4 - p_5 with minimal overlap, i.e., consisting only of the node p_3 .

Conceptually, the same decomposition principles can be applied to robot trajectory that is represented in the form of pose graphs; see Fig. 3. In graph-based SLAM, the linear systems to be solved arise from the Gauss-Newton

linearization of the nonlinear least-squares problem. The resulting system matrix has the form $A = H_{GN} = J^T W J$; see (2.8). The matrix A is sparse and exhibits a block structure corresponding to the robot poses. Throughout this paper, we will use minimal overlap as visualized in Fig. 3.

Mathematically, the local subdomain matrices in overlapping Schwarz are extracted from a global matrix using the subdomain restriction operators R_i from (3.1)

$$A_i = R_i A R_i^T, \quad i = 1, \dots, N.$$

In our context, the matrices A_i therefore correspond to the Gauss–Newton system restricted to a local subgraph of the pose graph. Note that the loop closure constraints, which, throughout this paper, we place in the overlap, introduce couplings between distant poses and therefore create connections between otherwise weakly coupled subdomains.

The one-level additive overlapping Schwarz preconditioner is then given by

$$M_{AS}^{-1} = \sum_{i=1}^N R_i^T A_i^{-1} R_i. \quad (3.2)$$

The operator M_{AS}^{-1} serves as a preconditioner for A and approximates the action of A^{-1} by combining the solutions of local subdomain problems.

In practice, the action of M_{AS}^{-1} consists of independent local solves on the subdomains, followed by an accumulation of the corrections. The inverse A_i^{-1} can either be computed using a sparse direct solver, or it is approximated.

From a parallel computing perspective, each subdomain typically corresponds to a process or a group of processes as in [24], or more generally to a thread or processing unit in a parallel implementation. The restriction operators R_i and their transposes then represent parallel communication or data movement patterns, e.g., in message passing (MPI) or shared-memory environments. Applying R_i corresponds to gathering local data, while applying R_i^T corresponds to scattering local corrections back to the global vector. The overlap determines the amount of communication or synchronization required.

Such parallel implementations arise naturally not only on distributed-memory systems, but also on shared-memory architectures and embedded multi-core platforms commonly used in robotic systems.

4 Equivalence between a Simplified SLAM Problem and a Finite Element Model

To further elucidate the structure and conditioning of the linear systems arising in pose graph optimization, we consider a minimal one-dimensional model problem. The purpose of this section is to establish an analogy between

a simplified SLAM problem and classical finite element discretizations. The model discussed here is deliberately elementary and serves as an explanatory tool; it is not identical to the nonlinear SLAM problem solved numerically in the experiments.

4.1 A Very Simple SLAM Problem

We consider a one-dimensional robot with scalar states $x_0, x_1, \dots, x_{10} \in \mathbb{R}$.

The robot moves from $x_0 = 0$ to $x_{10} = 10$ in ten steps of unit length (ground truth). We assume that the odometry measurements are systematically biased. Instead of the true step length 1, the robot measures

$$\tilde{\Phi}_{i,i+1} := 0.9, \quad i = 0, \dots, 9,$$

leading to the relations

$$x_{i+1} - x_i \approx 0.9$$

The robot recognizes both its start and end positions exactly (end-closure and boundary conditions). Hence, we impose the hard constraints

$$x_0 = 0, \quad x_{10} = 10.$$

4.2 Least-Squares Formulation

The SLAM problem is formulated as our least-squares minimization problem. For each odometry measurement, we define the residual

$$r_i(x) := (x_{i+1} - x_i) - \tilde{\Phi}_{i,i+1} = (x_{i+1} - x_i) - 0.9.$$

The objective functional is

$$\mathcal{J}(x) = \frac{1}{2} \sum_{i=0}^9 r_i(x)^2, \quad (4.1)$$

subject to the Dirichlet constraints on x_0 and x_{10} . Hence, our weight matrix W is chosen as the identity matrix.

4.3 Mechanical Interpretation and Equivalent Finite Element Formulation

Problem (4.1) is equivalent to a mechanical system consisting of a chain of linear axial bars: ten one-dimensional linear elastic bars; each bar has a rest length of 0.9; node 0 is fixed ($x_0 = 0$); node 10 is prescribed to $x_{10} = 10$.

The total elastic energy of the system is defined as

$$\mathcal{E}(x) = \sum_{i=0}^9 \frac{1}{2} ((x_{i+1} - x_i) - 0.9)^2,$$

which coincides with the SLAM objective functional. Thus, SLAM with end-closure can be interpreted as the computation of a mechanical equilibrium on a graph.

4.4 Resulting Sparse Linear System

The derivative of a single element energy

$$\frac{1}{2} ((x_{i+1} - x_i) - 0.9)^2$$

yields the local stiffness matrix

$$K^{(i)} = \begin{pmatrix} 1 & -1 \\ -1 & 1 \end{pmatrix},$$

acting on the degrees of freedom (x_i, x_{i+1}) .

Assembling all elements results in the global system

$$Kx = 0$$

with the (11×11) matrix

$$K = \begin{pmatrix} 1 & -1 & 0 & \cdots & 0 & 0 \\ -1 & 2 & -1 & \ddots & \vdots & \vdots \\ 0 & -1 & 2 & \ddots & 0 & 0 \\ \vdots & \ddots & \ddots & 2 & -1 & 0 \\ 0 & \cdots & 0 & -1 & 2 & -1 \\ 0 & \cdots & 0 & 0 & -1 & 1 \end{pmatrix}.$$

This is the classical tridiagonal matrix with stencil $(-1, 2, -1)$, which discretizes the one-dimensional Laplace operator.

The odometry measurements enter the formulation exclusively through the rest lengths of the bars. They do not generate a right-hand side.

Finally, Dirichlet boundary conditions are imposed in the classical strong form by matrix modification: rows corresponding to fixed degrees of freedom are set to zero and the diagonal entries are then set to one. The prescribed values appear on the right-hand side.

For

$$x_0 = 0, \quad x_{10} = 10,$$

this yields the modified system

$$\tilde{K}x = \tilde{b}$$

with

$$\tilde{K} = \begin{pmatrix} 1 & 0 & 0 & \cdots & 0 & 0 \\ -1 & 2 & -1 & \ddots & 0 & 0 \\ 0 & -1 & 2 & \ddots & 0 & 0 \\ \vdots & \ddots & \ddots & \ddots & 2 & -1 \\ 0 & 0 & 0 & -1 & 2 & -1 \\ 0 & 0 & 0 & \cdots & 0 & 1 \end{pmatrix}, \quad \tilde{b} = \begin{pmatrix} 0 \\ 0 \\ 0 \\ \vdots \\ 0 \\ 0 \\ 10 \end{pmatrix}.$$

The resulting linear system is non-symmetric but symmetry can be reestablished, e.g., to allow for conjugate gradients, by an elimination step. This removes the off-diagonal non-zero entries from the columns corresponding to the Dirichlet boundary. We obtain

$$\hat{K}x = \hat{b}, \quad x = (x_0, x_1, \dots, x_{10})^T,$$

with

$$\hat{K} = \begin{pmatrix} 1 & 0 & 0 & \cdots & 0 & 0 & 0 \\ 0 & 2 & -1 & \ddots & 0 & 0 & 0 \\ 0 & -1 & 2 & \ddots & 0 & 0 & 0 \\ \vdots & \ddots & \ddots & \ddots & -1 & 0 & \vdots \\ 0 & 0 & 0 & -1 & 2 & -1 & 0 \\ 0 & 0 & 0 & 0 & -1 & 2 & 0 \\ 0 & 0 & 0 & \cdots & 0 & 0 & 1 \end{pmatrix}, \quad \hat{b} = \begin{pmatrix} 0 \\ 0 \\ 0 \\ \vdots \\ 0 \\ 0 \\ 10 \\ 10 \end{pmatrix}.$$

The solution of the system is $x_i = i$, $i = 0, \dots, 10$. Mechanically, the excess length $10 - 9 = 1$ is distributed uniformly over all ten bars.

4.5 Relation to the Full SLAM Problem

The one-dimensional model discussed above is a linear, scalar, and purely local problem. In contrast, the SLAM problem solved in the numerical experiments:

- involves vector-valued unknowns,
- is nonlinear due to rotational components,
- leads to state-dependent Jacobian matrices,
- contains loop closure constraints inducing long-range couplings.

Nevertheless, the Gauss–Newton system matrices, see (2.7), arising in the full SLAM problem share essential properties with matrix (4.4): symmetry, positive definiteness after fixing the gauge, sparsity induced by local couplings, and a block structure corresponding to multi-component unknowns.

This analogy provides intuition for the use of domain decomposition methods in the SLAM-context and helps to explain the effectiveness of overlapping Schwarz preconditioners in this setting. It also motivates to consider other types of DDM from structural mechanics [20] as well.

5 Numerical Results and Discussion

5.1 Model Problem

To investigate the convergence of domain decomposition methods in SLAM, we consider the optimization of a pose graph SLAM problem in two dimensions, where the graph only contains the poses of the robots.

The odometry data are generated by adding Gaussian noise to the ground truth data, and optimization is subsequently performed on this noisy data. In our test case, the robot moves from the origin following a square trajectory, moving one unit to the right and turning left by 90° , repeating the motion until it returns to the starting point. We denote this movement around the unit square as *one loop*. Since the odometry is affected by noise, they do not correspond perfectly to the actual motion.

When the robot revisits the starting position, it recognizes that it has returned to a previously visited location, and a loop-closure edge is added to the pose graph; see Fig. 2. In our experiments, the weight matrix is $W_{ij} = 100I_3$ if the edge (i, j) corresponds to a loop closure, and $W_{ij} = 20I_3$ otherwise. The higher weight reflects the higher confidence assigned to loop closure constraints compared to the other measurements.

We solve the least-squares problem using Gauss–Newton, where the sparse systems from linearization are solved by conjugate gradients using additive overlapping Schwarz as a preconditioner. We use an absolute tolerance of

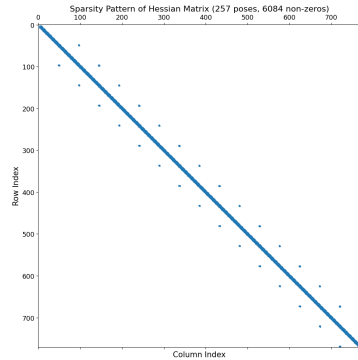


Fig. 4: Sparsity pattern of the system matrix. Loop closures introduce additional off-diagonal coupling visible in the sparsity.

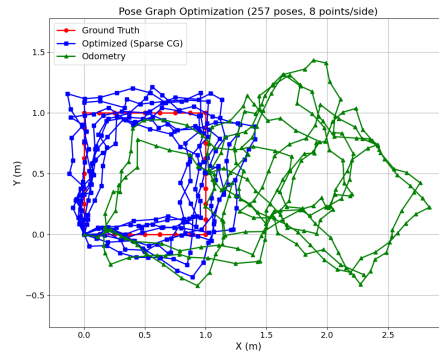


Fig. 5: Comparison of an optimized robot path with odometry and ground truth; 8 loops, 8 points per side.

$1e - 6$ for Gauss–Newton and a relative tolerance of $1e - 8$ for conjugate gradients. Since the inner conjugate gradient iteration uses a relative stopping criterion it is therefore less sensitive to the problem size. However, absolute stopping criteria in the outer nonlinear iteration may still lead to problem-size-dependent behavior.

In the subsequent text and tables, we will often write CG for conjugate gradients and GN for Gauss–Newton.

5.2 Overlapping Schwarz Preconditioner

In our experiments, each loop defines a subdomain for overlapping Schwarz. We use minimal overlap, where the overlap consists of three degrees of freedom. In our choice of the subdomains, the overlap includes the off-diagonal coupling introduced by the loop closures; see Fig. 4. In other words, the long range coupling introduced by the loop closure is placed in the subdomain overlap.

To evaluate the robustness and numerical scalability of this overlapping Schwarz preconditioner, the problem size is increased by increasing the number of loops (and thus the number of subdomains) traversed by the robot. We also consider the case where the number of odometry points on each side of the unit square is increased.

An example of the sparsity pattern of our system matrix is shown in Fig. 4. Here, 8 loops are traversed, with 8 points on each side of the unit square.

		No Preconditioner				Overlapping Schwarz			
		Iterations		Eigenvalues		Iterations		Eigenvalues	
Loops	Points/Side	GN	CG	Min	Max	GN	CG	λ_{\min}	λ_{\max}
4	4	5	153	0.30351	418.69	5	11	1.43	3.64
	8	5	274	0.08418	436.88	5	11	1.40	3.65
	16	6	511	0.02537	531.51	6	11	1.39	3.65
	32	5	1036	0.00593	444.48	5	11	1.38	3.67
	64	7	2146	0.00129	592.29	7	11	1.38	3.66
	128	12	3930	0.00039	586.15	12	10	1.40	3.67
8	4	5	206	0.18499	446.47	5	14	1.15	3.75
	8	6	385	0.06416	545.44	6	14	1.14	3.77
	16	6	706	0.02065	553.49	6	14	1.14	3.77
	32	6	1376	0.00544	475.42	6	13	1.15	3.76
	64	8	3029	0.00115	541.36	8	13	1.12	3.77
	128	10	5569	0.00028	562.67	10	12	1.14	3.75
16	4	5	329	0.0588	453.64	5	15	1.05	3.82
	8	5	551	0.02574	509.96	5	15	1.04	3.81
	16	6	992	0.00998	785.72	6	15	1.04	3.81
	32	6	2043	0.00308	646.82	6	14	1.04	3.81
	64	9	3790	0.00085	902.19	9	14	1.04	3.81
	128	11	9085	0.00016	2478.61	11	14	1.04	3.82
32	4	5	547	0.02459	460.74	5	16	1.02	3.83
	8	6	899	0.01053	630.25	6	16	1.03	3.83
	16	7	1557	0.00494	574.45	7	16	1.03	3.82
	32	7	2598	0.00225	854.45	7	16	1.01	3.82
	64	11	7298	0.00058	2893.99	11	15	1.02	3.82
	128	12	13706	0.00009	2415.83	12	15	1.00	3.81

Table 1: Comparison of the number of conjugate gradient (CG) iterations without preconditioner and when using the additive overlapping Schwarz preconditioner. We vary the number of loops and the points per side. The number of loops is identical to the number of overlapping subdomains, and the subdomain size increases with the points per side. The extremal eigenvalues λ_{\min} and λ_{\max} are estimated from the tridiagonal matrix generated by the Lanczos process.

Fig. 4 illustrates the sparsity of H and highlights the off-diagonal blocks resulting from the long range coupling introduced by the loop closures.

Fig. 5 show the solution of the nonlinear least square problem for the case where 8 cycles of unit squares have been traversed by the robot, with 8 odometry points taken at each side of the unit square. The solution of the least-squares problem converges to the same results with and without the use of our preconditioner.

		No Preconditioner				Overlapping Schwarz			
		Iterations		Eigenvalues		Iterations		Eigenvalues	
Loops	Points/Side	GN	CG	Min	Max	GN	CG	λ_{\min}	λ_{\max}
4	16	6	511	0.01969	1 161.41	6	11	1.39	3.65
8	16	6	706	0.01561	1 378.16	6	14	1.14	3.77
16	16	6	993	0.01014	1 949.00	6	15	1.04	3.81
32	16	7	1 557	0.00412	1 343.40	7	16	1.03	3.82
64	16	6	2 371	0.00146	1 436.35	6	16	1.01	3.83
128	16	10	6 371	0.00026	1 140.28	10	16	1.01	3.83

Table 2: Numerical scalability for an increasing number of subdomains. The number of additive Schwarz preconditioner CG iterations remains bounded for an increasing number of subdomains.

The numerical results obtained from the tests performed are presented in Table 1. In our numerical experiments, the robot traverses 4, 8, 16, and 32 loops. The number of loops coincides with the number of overlapping Schwarz subdomains, which means that at most 32 subdomains are used. Thus, this tests numerical scalability with respect to the number of subdomains (weak scalability). For each of these cases, we increase the number of odometry points at each side of the unit square until 128 points per side. This tests the numerical scalability for the case of increasing subdomain size. Note that in all cases minimal overlap is used.

In Table 1, we can see that the preconditioner drastically reduces the number of conjugate gradient (CG) iterations needed to reach convergence: While the number of unpreconditioned CG iterations increases to more than 10 000 Krylov iterations, the number of additive Schwarz preconditioned CG iterations always remains smaller or equal to 16.

In addition, the number of CG iterations does not increase significantly with the number of subdomains or with the subdomain size. This shows good numerical scalability for this particular test case, i.e., despite the increase in problem size, the number of CG iterations remains essentially constant, and the condition numbers $\lambda_{\max}/\lambda_{\min}$ of the preconditioned system stay bounded.

The numerical scalability with respect to the number of subdomains (and loops) is presented in Table 2 and Fig. 6. We observe, again, that the number of CG iterations remains bounded, when the additive Schwarz preconditioner is used. This is opposed to the case without preconditioner.

This result is obtained with a one-level method, i.e., without an explicit coarse space. While one-level overlapping Schwarz methods are in general not scalable for elliptic problems without a coarse space, scalability may still

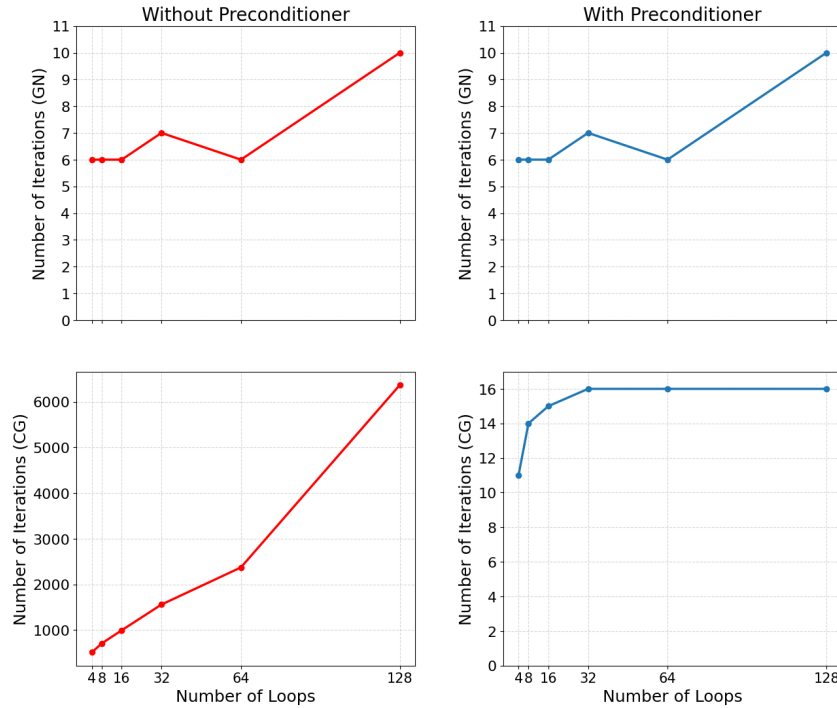


Fig. 6: Comparison of numerical scalability with and without using the overlapping Schwarz preconditioner by varying the number of loops traversed by the robot while the number of points at each side of unit square is kept constant at 16. The number of subdomains is always chosen equal to the number of loops.

occur for specific geometries, boundary conditions, or problem dimensions, as discussed for example in [25].

Let us briefly discuss the number of nonlinear iterations. The numerical results in Table 1 indicate that the number of Gauss–Newton iterations somewhat increases with the number of points per loop. To some extent, this may be a consequence of the absolute stopping criterion for Gauss–Newton, which is based on the standard Euclidean norm. However, for a fixed number of points per loop, the number of Gauss–Newton iterations appears to remain bounded as the number of loops increases. In Table 2, however, we observe an increase from 6 to 10 Gauss–Newton iterations when scaling to 128 loops. Further studies are necessary to determine whether the convergence of Gauss–Newton deteriorates for this problem as the number of loops grows.

6 Conclusion and Limitations

This paper presents first results indicating the potential effectiveness of an additive overlapping Schwarz preconditioner for a simple formulation of a pose graph SLAM problem. As a test case, we consider a robot traversing a unit square trajectory with an increasing number of loops and odometry points along each side of the square. In this setting, excellent weak scalability and a significant improvement in the conditioning of the problem were observed. The interpretation of a simplified SLAM problem as finite element discretization presented in this paper further provides intuition for why preconditioning techniques developed for discretized PDEs may also be applicable to SLAM problems. This observation motivates the exploration of domain decomposition methods as scalable solvers for large-scale SLAM optimization problems.

While the results presented in this paper are encouraging, several limitations of the current study should be acknowledged. The numerical experiments are conducted exclusively on a synthetic, highly regular test case, in which the robot repeatedly traverses a unit square trajectory. This setup implies a perfectly uniform graph structure, regularly spaced loop closures, and Gaussian measurement noise—conditions that are rarely encountered in real-world deployments. However, this test case was deliberately chosen to generate a controlled family of problem instances that allow systematic variation of the subdomain size and the number of subdomains. This enables us to investigate the sensitivity of the method with respect to the subdomain size as well as its numerical scalability with respect to the overall problem size, in particular whether the iteration counts remain bounded independently of the problem size.

Furthermore, the current experiments place loop closure constraints within the overlap region, which may contribute to the favorable results. Investigating other configurations will help clarify whether this choice is essential.

Future work will consider alternative nonlinear solvers such as Levenberg–Marquardt, as well as globalization and acceleration techniques in nonlinear optimization, including trust-region strategies and nonlinear domain decomposition methods. We will further validate the approach on established real-world benchmarks such as the KITTI or EuRoC datasets and study alternative decomposition strategies as well as different overlap sizes and their effect on the convergence behavior. Although a coarse problem was not required in the present example, more general SLAM problems may benefit from the inclusion of a coarse space tailored to the problem structure.

References

1. Frank Dellaert, Justin Carlson, Viorela Ila, Kai Ni, and Charles E Thorpe. Subgraph-preconditioned conjugate gradients for large scale SLAM. In *2010 IEEE/RSJ International Conference on Intelligent Robots and Systems*, pages 2566–2571. IEEE, 2010. <http://doi.org/10.1109/IRoS.2010.5650422>.
2. Jian He and Frank Dellaert. Incremental subgraph preconditioned conjugate gradient method for graph slam. In *Proceedings of the IEEE/RSJ International Conference on Intelligent Robots and Systems (IROS)*, pages 3934–3941. IEEE, 2014. <http://doi.org/10.1109/IRoS.2014.6942924>.
3. Sameer Agarwal, Noah Snavely, Steven M. Seitz, and Richard Szeliski. Bundle adjustment in the large. In *Proceedings of the European Conference on Computer Vision (ECCV)*, pages 29–42. Springer, 2010. http://doi.org/10.1007/978-3-642-15552-9_3.
4. Kurt Konolige, Giorgio Grisetti, Rainer Kümmerle, Wolfram Burgard, Benson Limketkai, and Regis Vincent. Efficient sparse pose adjustment for 2d mapping. In *2010 IEEE/RSJ International Conference on Intelligent Robots and Systems*, pages 22–29, 2010. <http://doi.org/10.1109/IRoS.2010.5649043>.
5. Rainer Kümmerle, Giorgio Grisetti, Hauke Strasdat, Kurt Konolige, and Wolfram Burgard. g2o: A general framework for graph optimization. In *Proceedings of the IEEE International Conference on Robotics and Automation (ICRA)*, pages 3607–3613. IEEE, 2011. <http://doi.org/10.1109/ICRA.2011.5979949>.
6. Cesar Cadena, Luca Carlone, Henry Carrillo, Yasir Latif, Davide Scaramuzza, José Neira, Ian Reid, and John J. Leonard. Past, present, and future of simultaneous localization and mapping: Toward the robust-perception age. *IEEE Transactions on Robotics*, 32(6):1309–1332, 2016. <http://doi.org/10.1109/TRo.2016.2624754>.
7. Hugh Durrant-Whyte and Tim Bailey. Simultaneous localization and mapping: Part i. *IEEE Robotics & Automation Magazine*, 13(2):99–110, 2006. <http://doi.org/10.1109/MRA.2006.1638022>.
8. Hugh Durrant-Whyte and Tim Bailey. Simultaneous localization and mapping: Part ii. *IEEE Robotics & Automation Magazine*, 13(3):108–117, 2006. <http://doi.org/10.1109/MRA.2006.1678144>.
9. Hugh Durrant-Whyte, David Rye, and Eduardo Nebot. Localization of autonomous guided vehicles. In Georges Giralt and Gerhard Hirzinger, editors, *Robotics Research*, pages 613–625. London, 1996. Springer London. http://doi.org/10.1007/978-1-4471-0765-1_69.
10. Josep Aulinas, Yvan Petillot, Joaquim Salvi, and Xavier Lladó. The SLAM problem: a survey. In *Artificial Intelligence Research and Development: Proceedings of the 11th International Conference of the Catalan Association for Artificial Intelligence*, pages 363–371. IOS Press, 2008. <http://doi.org/10.3233/978-1-58603-925-7-363>.
11. Bashar Alsadik and Samer Karam. The simultaneous localization and mapping (SLAM): An overview. *Journal of Applied Science and Technology Trends*, 2(2):147–158, 2021. <http://doi.org/10.38094/jastt204117>.
12. Weifeng Chen, Chengjun Zhou, Guangtao Shang, Xiyang Wang, Zhenxiong Li, Chonghui Xu, and Kai Hu. SLAM overview: from single sensor to heterogeneous fusion. *Remote Sensing*, 14(23):6033, 2022. <http://doi.org/10.3390/rs14236033>.
13. Andréa Macario Barros, Maugan Michel, Yoann Moline, Gwenolé Corre, and Frédéric Carrel. A comprehensive survey of visual SLAM algorithms. *Robotics*, 11(1):24, 2022. <http://doi.org/10.3390/robotics11010024>.
14. Leyao Huang. Review on LiDAR-based SLAM techniques. In *2021 International conference on signal processing and machine learning (CONF-SPML)*, pages 163–168. IEEE, 2021. <http://doi.org/10.1109/CONF-SPML54095.2021.00040>.
15. Giorgio Grisetti, Rainer Kümmerle, Cyrill Stachniss, and Wolfram Burgard. A tutorial on graph-based SLAM. *IEEE Intelligent Transportation Systems Magazine*, 2(4):31–43, 2011. <http://doi.org/10.1109/MITS.2010.939925>.

16. Andrea Toselli and Olof Widlund. *Domain decomposition methods—algorithms and theory*, volume 34 of *Springer Series in Computational Mathematics*. Springer-Verlag, Berlin, 2005. <http://doi.org/10.1007/b137868>.
17. Barry F. Smith, Petter E. Björstad, and William D. Gropp. *Domain decomposition. Parallel multilevel methods for elliptic partial differential equations*. Cambridge: Cambridge University Press, 1996. ISBN 9780521602860.
18. William D Gropp and David E Keyes. Domain decomposition methods in computational fluid dynamics. *International journal for numerical methods in fluids*, 14(2):147–165, 1992. <http://doi.org/10.1002/flid.1650140203>.
19. Pierre Gosselet and Christian Rey. Non-overlapping domain decomposition methods in structural mechanics. *Archives of computational methods in engineering*, 13(4):515, 2006. <http://doi.org/10.1007/BF02905857>.
20. Oliver Rheinbach. Parallel iterative substructuring in structural mechanics. *Archives of Computational Methods in Engineering*, 16(4):425–463, 2009. <http://doi.org/10.1007/s11831-009-9035-4>.
21. Alberto Corigliano, Martino Dossi, and Stefano Mariani. Domain decomposition and model order reduction methods applied to the simulation of multi-physics problems in MEMS. *Computers & Structures*, 122:113–127, 2013. <http://doi.org/10.1016/j.compstruc.2012.12.012>.
22. Bjoern Kiefer, Stefan Prüger, Oliver Rheinbach, and Friederike Röver. Monolithic parallel overlapping Schwarz methods in fully-coupled nonlinear chemo-mechanics problems. *Comput. Mech.*, 71(4):765–788, 2023. <http://doi.org/10.1007/s00466-022-02254-y>.
23. Axel Klawonn, Stephan Köhler, Martin Lanser, and Oliver Rheinbach. Computational homogenization with million-way parallelism using domain decomposition methods. *Comput. Mech.*, 65(1):1–22, 2020. <http://doi.org/10.1007/s00466-019-01749-5>.
24. Alexander Heinlein, Oliver Rheinbach, and Friederike Röver. Parallel scalability of three-level FROSch preconditioners to 220000 cores using the Theta supercomputer. *SIAM Journal on Scientific Computing*, 45(3):s173–s198, 2023. <http://doi.org/10.1137/21M1431205>.
25. Faycal Chaouqui, Gabriele Ciaramella, Martin J Gander, and Tommaso Vanzan. On the scalability of classical one-level domain-decomposition methods. *Vietnam Journal of Mathematics*, 46(4):1053–1088, 2018. <http://doi.org/10.1007/s10013-018-0316-9>.